Int. J. Heat Mass Transfer. Vol. 17, pp. 173–184. Pergamon Press 1974. Printed in Great Britain

NATURAL CONVECTION FLOW IN A FINITE, RECTANGULAR SLOT ARBITRARILY ORIENTED WITH RESPECT TO THE GRAVITY VECTOR

IVAN CATTON,* P. S. AYYASWAMY† and R. M. CLEVER‡
University of California, Los Angeles, California 90024, U.S.A.

(*Received* 13 *December* 1972 *and in revised form* 30 *June* 1973)

Abstract—Solutions to the stationary two-dimensional equations of motion governing natural convection flow of a large Prandtl number Boussinesq fluid contained in a differentially heated inclined rectangular slot have been obtained by the Galerkin method. The problem has been solved for perfectly conductive and adiabatic boundary conditions on the border strips. The range of parameters investigated include: Rayleigh numbers up to 2×10^6, aspect ratios from 0·1 to 20, and tilt angles from $-30°$ (bottom plate hotter) to $+75°$ (top plate hotter). These parameters describe both the conduction and boundary layer regimes. The computed flow distributions, including the appearance of multicellular flows, the temperature profiles, and the heat transfer predictions compare favorably with experimental results, and with other numerical studies.

INTRODUCTION

STEADY two-dimensional natural convection in an enclosed vertical rectangular cavity with horizontal temperature gradients has been the subject of many experimental, analytical and numerical studies. Comprehensive reviews of both the experimental and theoretical studies have been given by Ayyaswamy [1] and Hart [2]. As has been pointed out by both Ayyaswamy and Hart, there is a serious lack of information regarding the nature of the flow and the associated heat transfer rates for natural convection in inclined geometries.

While the vertical, rectangular cavity problem is in itself a challenging one, the generalized problem of tilted configurations poses a formidable task owing to the components of the gravitational field playing a rather significant role in the governing equations. The generalized problem is of great interest to physicists and engineers since it lends itself to the investigation of several limiting cases, such as geometries that are heated from below or from above, in addition to that of the differentially heated vertical slot.

The earliest analytical attack on the vertical geometry is that of Batchelor [3]. Gill [4] extends this work to clearly delineate the conduction and boundary layer regimes. The corresponding definitive experimental work, dealing with the nature of the flow mechanisms, is that of Elder [5, 6]. Eckert and Carlson [7] and Emery [8] have experimentally investigated the vertical slot problem and have presented heat transfer results extending from the conduction regime to large Rayleigh numbers. Poots [9], deVahl Davis [10], Rubel and Landis [11] and Quon [12] have approached this problem by numerical techniques and have also reviewed related numerical studies.

There have been studies of the effect of vertical boundaries in a layer of fluid heated from below by Segel [13], Krishnamurti [14], Davis [15] and Catton and Edwards [16].

Prandtl [17] has discussed the tilted configuration problem in the context of "mountain and valley winds". Gershuni [18] investigated the thermal stability of such thermally driven flows. However, the first and only systematic theoretical and experimental analysis of the effect of sloping boundaries on thermal convection is that of Hart [2]. Hart describes the base flow in a tilted slot essentially in terms of a parallel flow model with certain adjustable parameters. This description has enabled him to carry out the stability analysis of the flow. The adjustable parameters are carefully chosen to satisfy experimental observations. Hart, however, does not report averaged Nusselt number values. Dropkin and Somerscales [19] have presented some experimental data and correlations pertaining to the heat transfer coefficients for fluids confined between sloping boundaries. The range of their experimentation is limited to: (a) the bottom plate hotter configuration (vertical case excepted); (b) high Rayleigh numbers. The absence of an aspect ratio dependence in their final correlations for the Nusselt number and the assumptions of (a) the flow being turbulent in every case studied by them,

* Assistant Professor, Energy and Kinetics Department, School of Engineering and Applied Science.
† Postdoctoral Scholar, Institute of Geophysics and Planetary Physics.
‡ Postgraduate Research Enginer, Energy and Kinetics Department, School of Engineering and Applied Science.

and (b) a uniform hot wall temperature, have been questioned by Landis [20].

The great practical utility of heat transfer results for natural convection flows in tilted configurations has been the primary motivation for this work. In this paper, the Galerkin method is used to solve the coupled non-linear partial differential equations which govern the heat transmission in a closed rectangular cell having isothermal side walls and inclined at an angle θ to the vertical. The theory has been developed for a finite Prandtl number fluid flow but the equation set has been solved only in the limit of high Prandtl number. The boundary conditions on the border strips include both the cases of perfect conduction and perfect insulation. Several aspect ratios and Rayleigh number situations have been explored in order to understand the conduction and boundary layer regimes of natural convection flow in tilted geometries.

The method of attack used here has proven to be computationally simple, admirably suited for analyzing high parameter flow situations and less expensive in comparison to several other numerical schemes.

THEORETICAL FORMULATION

Governing equations

Consider a fluid space enclosed between two plane parallel boundaries inclined at an angle θ to the vertical and by two border strips of length $2h$ and distance $2H$ apart as shown in Fig. 1. Let T_H and $-T_H$ be the absolute temperatures of the hot and cold walls respectively. For an incompressible fluid contained in such a space the governing equations of motion are

$$\nabla \cdot \boldsymbol{v} = 0, \tag{1}$$

$$\rho_0 \frac{\mathrm{D}\boldsymbol{v}}{\mathrm{D}t} = -\nabla p + \mu \nabla^2 \boldsymbol{v} + \rho \boldsymbol{g}, \tag{2}$$

$$\frac{\mathrm{D}T}{\mathrm{D}t} = \kappa \nabla^2 T, \tag{3}$$

$$\rho = \rho_0(1 - \alpha T), \tag{4}$$

where D/Dt is the material derivative, μ, the dynamic viscosity, ρ, the density, ρ_0 is the density at the average fluid temperature, κ the thermal diffusivity, α, the coefficient of thermal expansion and $\boldsymbol{g}$ the gravitational acceleration vector.

Non-dimensionalize equations (1)–(4) by measuring distances, time, velocity, temperature and pressure in terms of h, h^2/ν, $g\alpha\beta h^3/\nu$, βh and $\rho_0 \beta \alpha g h^2$ respectively. Here ν, is the kinematic viscosity and β, the temperature gradient. Boussinesq approximation enables us to write equations (1)–(4) for steady flow as follows:

$$\nabla \cdot \boldsymbol{v} = 0, \tag{5}$$

$$G^*(\boldsymbol{v} \cdot \nabla)\boldsymbol{v} = -\nabla p + \nabla^2 \boldsymbol{v} - T\boldsymbol{n}, \tag{6}$$

$$G^*(\boldsymbol{v} \cdot \nabla)T = \frac{1}{P} \nabla^2 T, \tag{7}$$

where $G^*(= g\alpha\beta h^4/\nu^2)$ is the Grashof number based on the cavity half width, $P(= \nu/\kappa)$ the Prandtl number and $\boldsymbol{n}$ is the unit vector normal. In this work only two-dimensional motion is considered. Hence

$$\boldsymbol{v} = \boldsymbol{i}u + \boldsymbol{k}w \tag{8}$$

where u and w are the components of velocity and $\boldsymbol{i}$ and $\boldsymbol{k}$ are unit vectors in the x and z directions respectively.

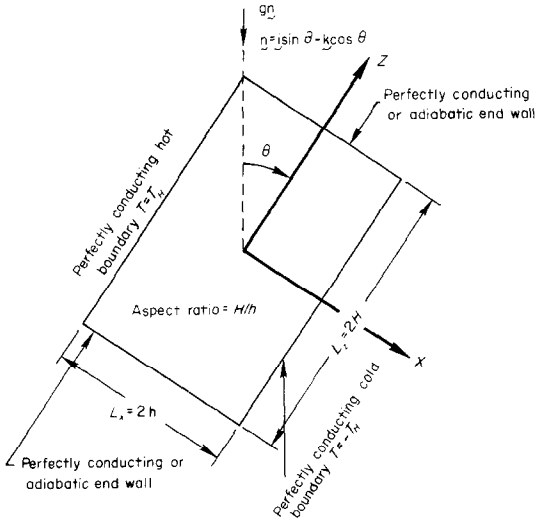

FIG. 1. Geometry and coordinate system of the rectangular region.

Boundary conditions

Set $A = (H/h)$ to denote the aspect ratio. For rigid walls enclosing the fluid the velocity boundary conditions are

$$\begin{aligned} u(\pm 1, z) &= w(\pm 1, z) = 0, \\ u(x, \pm A) &= w(x, \pm A) = 0. \end{aligned} \tag{9}$$

The temperature boundary conditions on the isothermal walls are

$$T(\pm 1, z) = \mp 1 \tag{10}$$

and the conditions on the border strips would be

$$T(x, \pm A) = -x \tag{11}$$

for perfectly conducting strips, while

$$\left.\frac{\partial T}{\partial z}\right|_{(x, \pm A)} = 0 \tag{12}$$

for perfectly insulating strips.

Galerkin method of solution

Represent u, w and T by series sums as follows:

$$u(x, z) = \sum_{m=1}^{N} B_m u_m(x, z), \tag{13}$$

$$w(x, z) = \sum_{m=1}^{N} B_m w_m(x, z), \tag{14}$$

$$T(x, z) = -x + \sum_{m=1}^{N} A_m f_m(x, z), \tag{15}$$

where A_m and B_m are undetermined Galerkin coefficients and u_m, w_m and f_m are trial functions chosen to satisfy the appropriate boundary conditions of the problem. N is a finite number. Let $\boldsymbol{v}_n = \boldsymbol{i}u_n + \boldsymbol{k}w_n$ and f_n represent one term of the series representations above for $\boldsymbol{v}$ and T respectively. The interior method is used by taking the vector dot product of the momentum equation (6) with $\boldsymbol{v}_n$ and scalar multiplication of energy equation (7) by f_n and volume integrating the resulting equations. Simplification of the system yields

$$G^* \int_\tau \boldsymbol{v}_n \cdot [\boldsymbol{v} \times (\nabla \times \boldsymbol{v})] \mathrm{d}\tau - \int_\tau \nabla \boldsymbol{v}_n : \nabla \boldsymbol{v} \, \mathrm{d}\tau - \int_\tau \boldsymbol{v}_n \cdot T\boldsymbol{n} \mathrm{d}\tau = 0$$

$$n = 1, 2, \ldots N \tag{16}$$

and

$$\int_\tau f_n \nabla^2 T \mathrm{d}\tau - R^* \int_\tau f_n (\boldsymbol{v} \cdot \nabla) T \mathrm{d}\tau = 0$$

$$n = 1, 2, \ldots N \tag{17}$$

where τ represents volume and R^* the Rayleigh number based on cavity half width ($= G^* \cdot P$).

Introducing the series representations, equations (13)–(15), of the dependent variables into equations (16) and (17) the following coupled set of matrix equations for the undetermined Galerkin coefficients are obtained

$$L^{(1)}_{nm} B_m + L^{(2)}_{nm} A_m + \frac{R^*}{P} \sum_k L^{(1)}_{nmk} B_k B_m = L^{(3)}_n, \tag{18}$$

$$R^* L^{(4)}_{nm} B_m + L^{(5)}_{nm} A_m - \sum_k R^* L^{(2)}_{nmk} B_k A_m = 0, \tag{19}$$

where the standard summation convention is used and the coefficient matrices are defined as follows:

$$L^{(1)}_{nm} = -\int_\tau (\nabla \boldsymbol{v}_n : \nabla \boldsymbol{v}_m) \mathrm{d}\tau,$$

$$L^{(2)}_{nm} = \int_\tau (w_n \cos\theta - u_n \sin\theta) f_m \mathrm{d}\tau,$$

$$L^{(1)}_{nmk} = \int_\tau (u_n w_m - w_n u_m) \left(\frac{\partial w_k}{\partial x} - \frac{\partial u_k}{\partial z}\right) \mathrm{d}\tau,$$

$$L^{(3)}_n = \int_\tau (w_n \cos\theta - u_n \sin\theta) x \mathrm{d}\tau, \tag{20}$$

$$L^{(4)}_{nm} = \int_\tau f_n u_m \mathrm{d}\tau, \qquad L^{(5)}_{nm} = \int_\tau f_n \nabla^2 f_m \mathrm{d}\tau,$$

$$L^{(2)}_{nmk} = \int_\tau f_n \left(u_k \frac{\partial f_m}{\partial x} + w_k \frac{\partial f_m}{\partial z}\right) \mathrm{d}\tau.$$

High Prandtl number limit

In the limit of high Prandtl number, equation (18) reduces to

$$L^{(1)}_{nm} B_m + L^{(2)}_{nm} A_m = L^{(3)}_n. \tag{21}$$

Solving this for B_m yields

$$B_m = -L^{(1)-1}_{ml} L^{(2)}_{lq} A_q + L^{(1)-1}_{ml} L^{(3)}_l. \tag{22}$$

Substituting equation (22) into equation (19) and rearranging results in

$$M_{nmk} A_k A_m + D_{nm} A_m = E_n, \tag{23}$$

where

$$M_{nmk} = R^* L^{(2)}_{nmp} L^{(1)-1}_{pl} L^{(2)}_{lk}, \tag{24}$$

$$D_{nm} = L^{(5)}_{nm} - R^* [L^{(4)}_{np} L^{(1)-1}_{Pl} L^{(2)}_{lm} + L^{(2)}_{nmp} L^{(1)-1}_{Pl} L^{(3)}_l], \tag{25}$$

and

$$E_n = -R^* L^{(4)}_{nm} L^{(1)-1}_{nl} L^{(3)}_l. \tag{26}$$

Equation (23) can now be solved by the Newton–Raphson technique for the coefficients A_m and B_m. To evaluate the matrix elements the trial functions u_m, w_m and f_m must be specified.

Choice of the trial functions

By choosing suitable expansions for u, w and f it is possible to obtain good approximate solutions. This choice is important in as much as a truncation at some finite number N is required in any practical calculation. It is also necessary to use several sets of trial functions and combinations thereof in order to accommodate all possible velocity and temperature field variations in the fluid space.

The trial-velocity sequence $\boldsymbol{v}$ is constructed from a

linear combination of orthogonal basis vectors given by

$$\mathbf{v}_m = \text{curl}\,\{\psi_m(x, z)\mathbf{j}\}, \tag{27}$$

where $\mathbf{j}$ denotes the unit vector in the y direction and ψ_m is an arbitrary defining scalar field. In a system of cartesian coordinates (x, z), the components of $\mathbf{v}_m$ are

$$u_m = -\frac{\partial \psi_m}{\partial z}, \qquad w_m = \frac{\partial \psi_m}{\partial x}. \tag{28}$$

Even and odd scalar fields that satisfy the boundary conditions are

$$\psi_m^{(e)} = C_{J_m}(x)\, C_{k_m}(z/A), \tag{29}$$

$$\psi_m^{(o)} = S_{J_m}(x)\, S_{k_m}(z/A), \tag{30}$$

where

$$C_{J_m}(x) = \frac{\cosh(\lambda_{J_m} x)}{\cosh(\lambda_{J_m})} - \frac{\cos(\lambda_{J_m} x)}{\cos(\lambda_{J_m})}, \tag{31}$$

$$S_{J_m}(x) = \frac{\sinh(\mu_{J_m} x)}{\sinh(\mu_{J_m})} - \frac{\sin(\mu_{J_m} x)}{\sin(\mu_{J_m})} \tag{32}$$

are the beam functions and the superscripts e and o indicate even and odd. The roots λ and μ are selected to make the derivative zero at $x = \pm 1$. The roots tabulated in appendix V of Chandrasekhar [21] are twice the value needed here due to the different scaling of the problem.

The trial functions selected for the temperature field are selected to have the same symmetry as the vertical velocity component. This selection is made based on the symmetry implied by the momentum equation. Sets of trial functions are chosen for both types of slot end walls. The trial functions are

$$f_m^{(e)}(x, z) = \sin(J_m \pi x) \cos\left((2k_m - 1 - \alpha)\frac{\pi}{2} z/A\right) \tag{33}$$

and

$$f_m^{(o)}(x, z) = \cos\left((2J_m - 1)\frac{\pi}{2} x\right) \sin\left((2k_m - \alpha)\frac{\pi}{2} z/A\right) \tag{34}$$

where $\alpha = 0$ for perfectly conducting end walls and $\alpha = 1$ for adiabatic end walls. In this case the superscripts correspond to equations (29) and (30).

Nusselt number calculation

The thermal quantity measured experimentally is the rate of heat transfer through the cold boundary. If this rate is Q heat units per second per unit depth of boundary in the y direction, then a dimensionless quantity describing the heat transfer is the Nusselt number

$$Nu = \frac{Q}{k(T_{\text{hot}} - T_{\text{cold}})} \tag{35}$$

where k is the thermal conductivity of the fluid. Here, the equivalent definition for the Nusselt number is,

$$Nu = -\frac{1}{2A}\int_{-A}^{+A} \left(\frac{\partial T}{\partial x}\right)\Big|_{x=+1} \mathrm{d}z. \tag{36}$$

SOLUTION PROCEDURE FOR THE MATRIX EQUATION

Consider solving,

$$F_n(A_k) = M_{nmk} A_k A_m + D_{nm} A_m - E_n = 0. \tag{37}$$

For a low enough Rayleigh number R we have

$$A_i^2 \ll A_i \tag{38}$$

and A_m obtained as a solution to the linear equation

$$D_{nm} A_m = E_n \tag{39}$$

is a good first approximation. Further improvement of this A_m at low Rayleigh numbers can now be effected by expanding equation (23) in a Taylor series about the first approximation. This expansion yields for the nth iterate

$$A_i^{(n+1)} = A_i^{(n)} - G_{ij}^{-1} F_j^{(n)} \tag{40}$$

where

$$F_i^{(n)} = M_{ijk} A_k^{(n)} A_j^{(n)} + D_{ij} A_j^{(n)} - E_i \tag{41}$$

and

$$G_{ij} = (M_{ijk} + M_{ikj}) A_k^{(n)} + D_{ij}. \tag{42}$$

The iterative procedure is continued until a desired convergence criterion is satisfied. In this work this criterion was

$$\left|\frac{F_k^{(n+1)}(A_k) - F_k^{(n)}(A_k)}{F_k^{(n)}(A_k)}\right| \lesssim 10^{-6}. \tag{43}$$

It is found that faster convergence is obtainable at higher Rayleigh numbers when the preceding lower Rayleigh number solution is used as a first guess in equation (23) instead of using the linearized solution given by equation (39) to start the procedure each time.

RESULTS AND DISCUSSION

Solutions to equation (23) have been obtained for Rayleigh numbers based on cavity width ($R = g\alpha\beta(2h)^4/\nu\kappa = 16R^*$) up to 2×10^6, aspect ratios (height/width) varying from 0·2 to 20, angles of tilt

from $-30°$ to $+75°$ (negative angles imply lower plate hotter) and for both adiabatic and perfectly conducting end wall conditions. Successive approximations were carried out for increasing values of N up to $N = 32$. Due to physical limitations of computational core storage (IBM 360/91), solutions for $N > 32$ were not run.

With $N = 32$ difficulties first arose for perfectly conducting end walls and large angles of tilt as well as with larger aspect ratios. Only those cases which yielded meaningful results have been presented. Where possible, the results are compared with those of other investigators. The agreement is found to be very good at low R. At high R, the true solution (or solutions) is not precisely known, but the qualitative behavior seems to be good. Suffice it to say, that for high R, more precise heat transfer results and flow characteristics can be obtained for values of $N > 32$.

Heat transfer results

The averaged Nusselt number for a rectangular region with insulating end walls and $\theta = -30°$, $-20°$ and $0°$ is given in Fig. 2. Solutions for tilt angles $\theta < -30°$ have not been obtained. For larger negative tilt angles, longitudinal roll instabilities (see, Hart [2] or Kurzweg [22]) manifest themselves at small $R(R_c \gtrsim 1707/\sin|\theta|$, for $\theta < 0°)$, which necessitate a fully three-dimensional study of the governing equations before meaningful results can be obtained in this region. Admittedly, in the limit of an infinite Prandtl number fluid flow one can speculate that these instabilities would occur at somewhat higher Rayleigh numbers in comparison to those observed for a finite Prandtl number situation by Hart. Thus, it might be argued that meaningful two-dimensional solutions could be obtained for comparatively smaller tilt angles than can be done in the case of a finite Prandtl number fluid flow situation. To be on the conservative side of the foregoing situation, it was decided that $\theta < -30°$ not be investigated. For $\theta = -30°$, a comparison with the experimental findings of Dropkin and Somerscales [19] is possible. However, there seems to be a discrepancy between the results to the extent that the slope of results presented in [19] is large compared with those obtained in this work. Such a discrepancy seems attributable to a change in aspect ratio in order to effect a change in Rayleigh number as is often done in experimental work. It should be noticed that decreasing the aspect ratio (for large enough aspect ratios) at constant Rayleigh number effects an increase in the Nusselt number. Further, with smaller aspect ratios (< 1) the results exhibit a decreased heat transport with decreasing aspect ratio. A noteworthy feature is that for both $\theta = -20°$ and $\theta = -30°$, excepting for a small change in magnitude, the heat transfer results remain essentially the same.

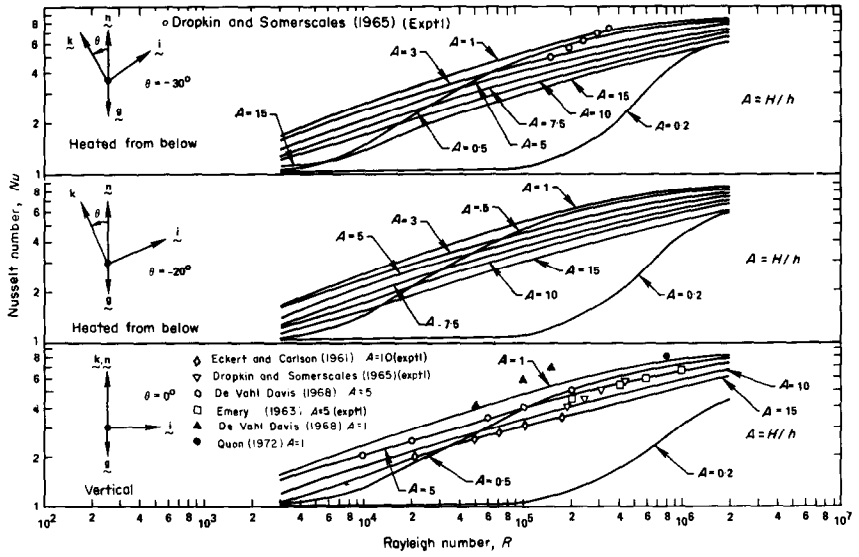

FIG. 2. Heat transfer across a two-dimensional rectangular region with insulating end walls for tilt angles $\theta = -30°, -20°, 0°$.

As stated earlier, the vertical configuration has

been the subject of numerous investigations. Several comparisons with the present work are possible and Fig. 2 shows results reported by related studies. The experimental results of Emery [8] compare very well while those of Dropkin and Somerscales [19] still show some discrepancy. The present results somewhat overpredict the values measured by Eckert and Carlson [7] at an aspect ratio of 10 with air ($P = 0{\cdot}7$) as the confined fluid. The over-prediction is perhaps due to the infinite Prandtl number assumption made in this analysis. Quon [12] has demonstrated that an infinite Prandtl number analysis is invalid for Prandtl numbers of this order. Comparisons with the numerical results reported by deVahl Davis [10] show agreement for an aspect ratio of 5 while those for a square cavity do not agree as well. The preliminary work done by Denny [23] using a finer grid spacing in a similar numerical investigation at unity aspect ratio has indicated that perhaps the disagreement is attributable to inaccuracies associated with deVahl Davis' choice of grid spacing. Quon [12] has obtained a single value for the Nusselt number at a Rayleigh number of 8×10^5, and an aspect ratio of one. The results presented in this work are thought to be possibly less accurate to the extent that for calculations at large Rayleigh numbers ($\sim O(10^6)$) the number of terms ($N = 32$) used in the Galerkin expansion are not quite sufficient.

Figure 3 presents results for a rectangular region with insulating end walls and $\theta = 30°$, 60° and 75°. As the angle increases, the effect of changing the aspect ratio is rather pronounced. For aspect ratios less than unity the results separate further with increasing angles of inclination. The results for the low aspect ratio cases indicate that with decreasing aspect ratio (for low enough aspect ratios), the convective heat transport is significantly decreased.

Heat transfer results for a rectangular region with perfectly conducting end walls, at $\theta = 0°$, 30° and 60°, are presented in Fig. 4. At $\theta = 0°$ and 30° the results for perfectly conducting end wall configurations show decreased heat transfer compared to those of adiabatic end walls. As would be expected, this effect is much more pronounced at low aspect ratios. However, at $\theta = 60°$ there is a reversal of this effect and, for particular values of A, the heat transfer is higher for the case of perfectly conducting end walls. Examination of local heat transport (see Fig. 5) on the heated wall shows this effect. For large aspect ratios ($A \geqslant 5$) and $\theta = 0°$, the local heat transport is essentially the same for both types of end walls, except near these boundaries. As the angle of tilt is increased, the differences become more noticeable. For $\theta = 0°$ and unit aspect ratio the results for perfectly conducting walls fall below those for adiabatic end walls (see Fig. 5b), whereas for large positive angles, $\theta = 60°$, this is reversed (see Fig. 5d). This is due to the more pronounced thermal interaction at the perfectly conducting boundaries as the tilt angle is increased. For small aspect ratio ($A = 0{\cdot}2$), within the range of

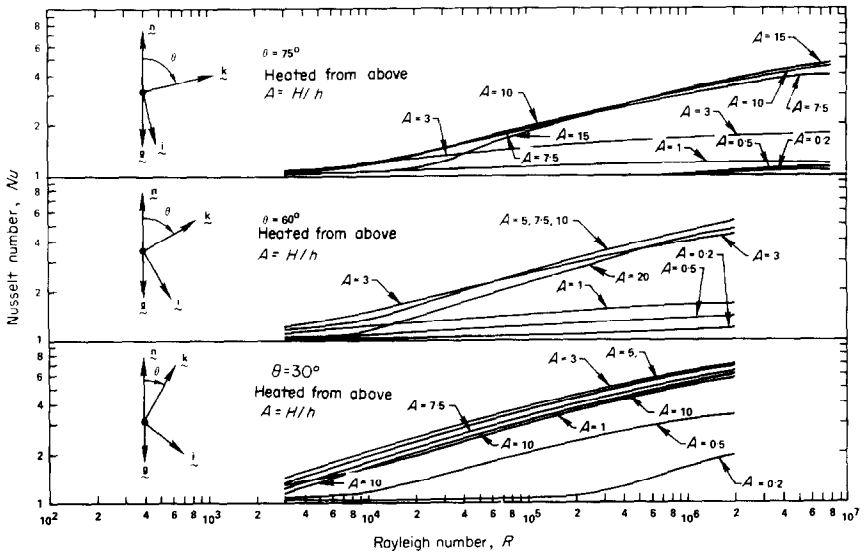

FIG. 3. Heat transfer across a two-dimensional rectangular region with insulating end walls for tilt angles $\theta = 30°$, 60°, 75°.

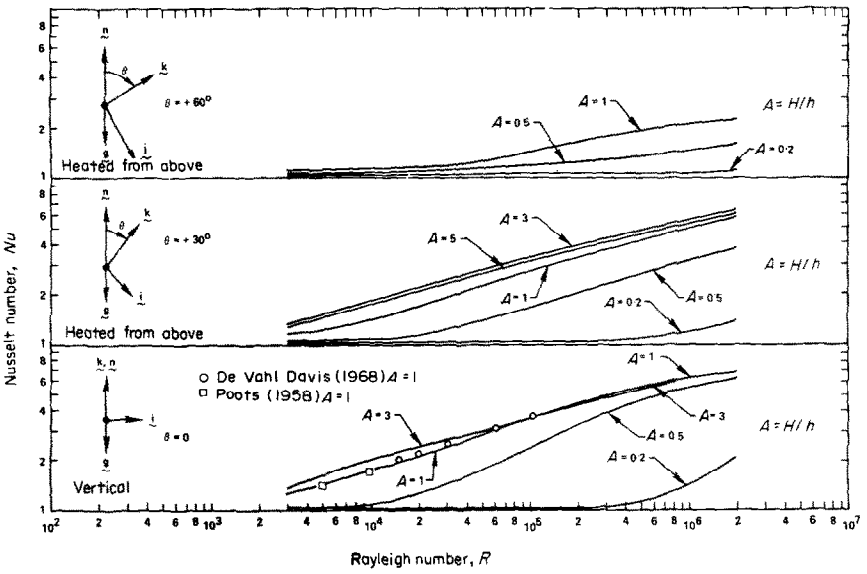

FIG. 4. Heat transfer across a two-dimensional region with perfectly conducting end walls for tilt angles $\theta = 0°, 30°, 60°$.

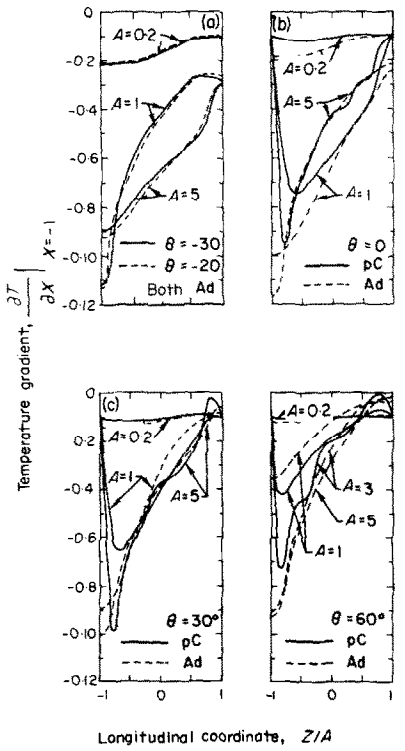

FIG. 5. Temperature gradient at the hot wall for $R = 300\,000$.

parameters investigated in this work, adiabatic end walls allow greater heat transport. Further, the effect of end walls is much more sensitive to the angle of tilt in this case.

Comparison with deVahl Davis [10] and Poots [9], for $\theta = 0°$ and $A = 1$, is shown in Fig. 4. The comparisons are good and might lead one to speculate that finite difference procedures have better convergence properties for perfectly conducting end walls than for insulating end walls. However, even if such convergence properties hold true for $\theta = 0°$, it seems unlikely that similar properties exist for large tilt angles. For both methods this is due to numerical difficulties inherent in accommodating thin boundary layer regions adjacent to perfectly conducting end walls.

Some local Nusselt number results at a Rayleigh number of 3×10^5 are shown in Fig. 5. Generally, for both positive and negative angles of tilt there is a decrease in the local Nusselt number, the effect for positive angle (heated from above) being greater. The effect of negative angle of tilt is somewhat compensated in the case of adiabatic end walls since the heat transport at the top of the heated wall is increased (the top is denoted by $z/A = 1$). For positive angles a decrease in the heat transport at the top is observed. This is thought to be due to the density stratification causing a relatively stagnant, constant temperature region in the corner adjacent to the heated wall. The

essential difference between the transport mechanisms in this region for perfectly conducting and adiabatic end wall cases is due to the onset of secondary flow for large enough R in the former case. The driving mechanism for this secondary flow seems clear. The trend toward thermal stratification causes an adverse temperature gradient adjacent to the perfectly conducting end wall. As in the classical Benard problem, this adverse temperature gradient seems likely to cause instability to secondary flow. Although it is not clear whether or not this secondary flow would be three-dimensional, the presence of such an instability in relatively constant temperature region would perhaps not significantly effect the overall heat transport. Due to this boundary effect it seems probable that, if and when instability to a three-dimensional flow does occur, it will occur at a lower R in the case of perfectly conducting end walls.

Temperature field

Typical temperature profiles at the cavity midheight and cavity center-plane, for a Rayleigh number of 3×10^5, are shown in Figs. 6 and 7. Due to the centro-symmetry property of the solutions (about $x = z = 0$), only the profiles for the left hand half at midheight (heated wall), and upper half at the centerplane are shown.

At the cavity midheight the trend toward pure conduction is indicated for larger tilt angle, and small aspect ratio. Near $\theta = 0°$ the deviation from conduction is greatest for unit aspect ratio, while for large tilt angle it is greatest for larger aspect ratio. As the results for Nusselt number indicate, the overall effect of thermal end wall conditions is most pronounced for large tilt angles and small aspect ratio. For $A \geq 3$ all of the results in Fig. 6 show larger deviation from conduction when the end wall is insulating. For $A \leq 1$, a reversal of this effect is observed as the angle of tilt is increased. Again, this is due to increased thermal interaction between the end and side walls as the angle of tilt is increased in the case of perfectly conducting end walls.

The trend toward vertical, thermal (i.e. density) stratification is shown in Fig. 7. Hart [2] discusses this stratification for large aspect ratio. In his approximate stability analysis he assumes a parallel flow model with constant longitudinal temperature gradient (near the midheight), and reasonably accurately predicts transition. The results presented here do indicate a trend toward this type of stratification for large aspect ratio; they are however, not conclusive. More accurate solutions, using $N > 32$, are necessary to assess the accuracy of Hart's assumption.

In the core, the vertical thermal stratification is

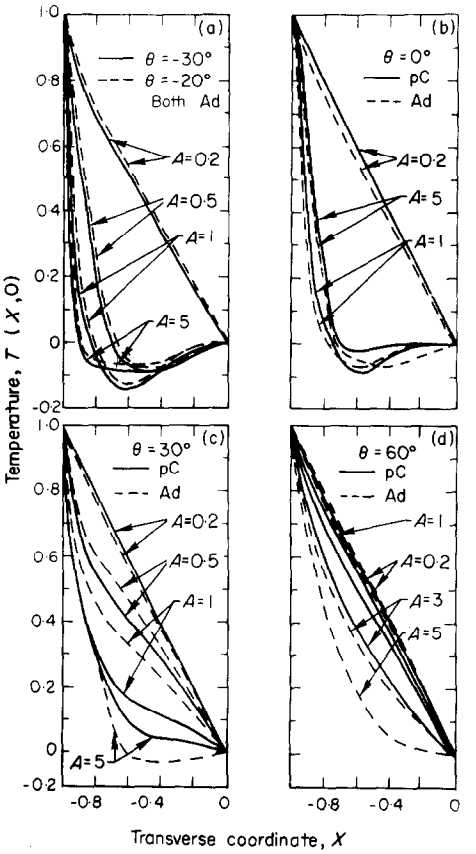

FIG. 6. Temperature at the cavity midheight, $z = 0$, for $R = 300\,000$.

more pronounced for aspect ratios near one, except for large tilt angles, where an aspect ratio of three shows it to be the largest. There seems to be a trend towards increasing longitudinal temperature gradient proceeding upward from midheight as aspect ratio is increased. This effect is significant at $\theta = 0°$, where $A = 1$ shows moderate increase and $A = 5$ shows substantial increase. At $\theta = 30°$, $A = 1$ shows a monotonically decreasing gradient, as does $A = 3$ at $\theta = 60°$, for the case of adiabatic end walls.

When the end walls are perfectly conducting, in most cases, the amount of thermal stratification is considerably less, although greater changes in gradient are present throughout the core region. Also, with increasing aspect ratio there exists a thin, adverse temperature gradient (thermal boundary layer region) near the end walls. This gradient is further increased with angle of tilt. The magnitude of the "boundary layer Rayleigh number" for various aspect ratios has not been presented. It is thought that the number of terms necessary to accurately predict

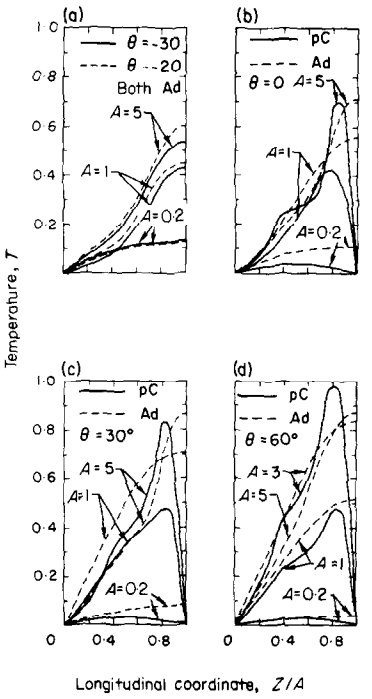

FIG. 7. Temperature at the cavity midplane, $x = 0$, for $R = 300\,000$.

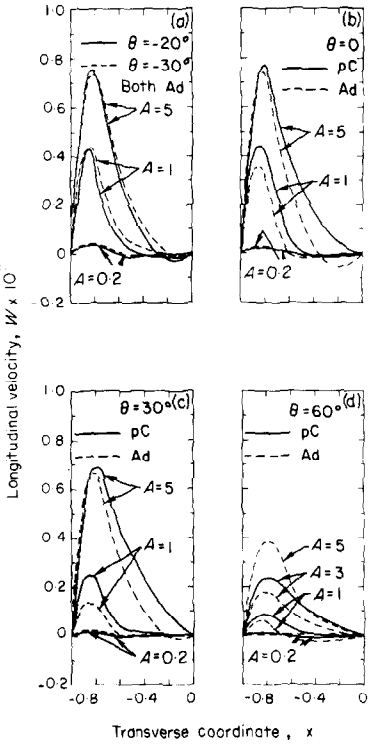

FIG. 8. Longitudinal velocity, w, at the cavity midheight, $z = 0$, for $R = 300\,000$.

these quantities for large aspect ratio (R_δ is proportional to δ^3) exceeds $N = 32$. In any case, as previously stated, the effect of such an instability on the average heat transport is probably small.

Velocity fields

The longitudinal (w) and transverse (u) velocity components at the cavity midheight ($z = 0$), and centerplane ($x = 0$) for a Rayleigh number of 3×10^5, are shown in Figs. 8–11. Here again, due to the centrosymmetry property, only fields on one half of the plane are presented.

For aspect ratios of order one or smaller, the existence of a velocity boundary layer near the heated wall is noticeable. This is most evident for the case $\theta = 0°$ and $A = 1$ (see Fig. 8). As the aspect ratio is increased, the profile approaches the classical "cubic velocity profile" (within the two-dimensional, large P imposition) for all tilt angles. As discussed previously, these do not necessarily represent physically realizable solutions of the equations of motion for $\theta < 0°$ (see Hart [2]). For larger R it seems likely (by examination of smaller R results) that the boundary layer effects should be greatest for smaller aspect ratios. Except for $A = 0{\cdot}2$, the results with perfectly conducting end walls show larger longitudinal velocity component at $z = 0$ than do those with adiabatic end walls, the difference increasing with tilt angle. Here again, thermal interaction between the side and the perfectly conducting end walls increases with tilt angle, even though the flow magnitude decreases with tilt angle for both perfectly conducting and adiabatic end walls.

With reference to Fig. 8, a longitudinal flow reversal near the cavity center may be noticed, this reversal being greater for adiabatic end wall conditions. However, with increasing tilt angles (for the parameters investigated here) the flow is less prone to flow reversals and in fact, the reversed flow is at most an order of magnitude smaller than the primary flow. The character of the longitudinal velocity component at the centerplane (see Fig. 9) indicates the likely formation of a secondary flow together with an increasingly skewed velocity field as angles of tilt are increased. These effects are quite large for large aspect ratios and large angles of tilt. The perfectly conducting end wall conditions compared to the adiabatic serve to inhibit these effects for smaller aspect ratios and tilt angles, while for larger aspect ratios and tilt angles the opposite seems to hold true.

The character and magnitude of the transverse velocity component at the centerplane is highly

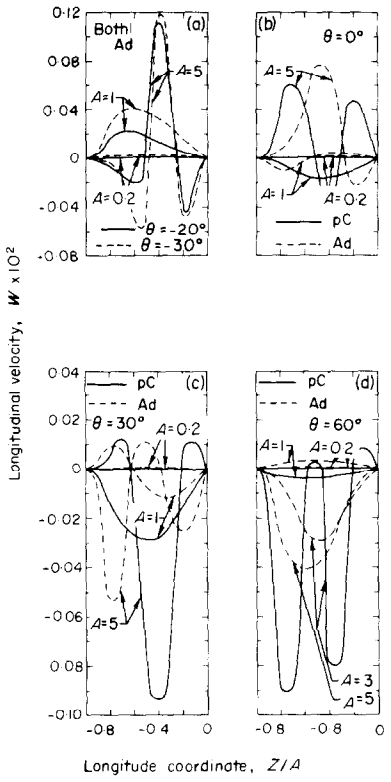

FIG. 9. Longitudinal velocity, w, at the cavity midplane, $x = 0$, for $R = 300000$.

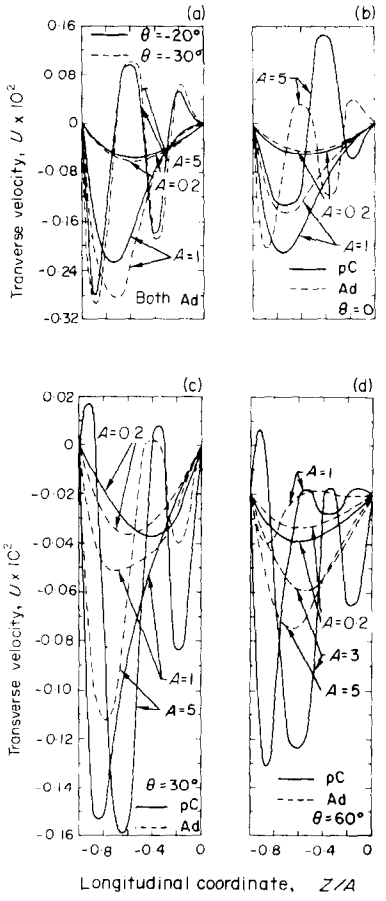

FIG. 10. Transverse velocity, u, at the cavity midheight, $x = 0$, for $R = 300000$.

dependent on the parameters of the problem. For tilt angles near vertical, transverse flow reversal at the midplane exists at large aspect ratio, for both end wall conditions (see Fig. 10). At large aspect ratio, the secondary flow appears in the interior with a vertical cell wavelength of approximately one third the cavity height. As the angle of tilt is increased the magnitude of the velocity component decreases, and the character of the flow depends, to a much larger extent, on the thermal end wall conditions. At $\theta = 60°$, for $A = 1$ and perfectly conducting end wall conditions, a distinct multicellular flow exists. For adiabatic end walls, such a distinct flow reversal is not noticeable under similar conditions. The transverse velocity component at midheight (Fig. 11) seems less likely to lead to a multicellular flow than does the longitudinal component at the centerplane. An examination of the magnitude of the transverse component, however, reveals an increasingly skewed velocity field with increasing tilt angles. It can be conjectured from a study of these effects that a distinct transverse wavelength cellular motion is unlikely at any aspect ratio, as contrary to the likelihood of the longitudinal wavelength cellular motion for large aspect ratios.

SUMMARY AND CONCLUSIONS

Solutions to the stationary, two-dimensional equations of motion governing large Prandtl number Boussinesq fluid flow in rectangular geometries have been obtained. Several aspect ratios, Rayleigh numbers, and angles of tilt have been investigated for both perfectly conducting and adiabatic end wall boundaries.

As previously stated, the motivation for this work stems largely from a desire to obtain heat transport results in inclined geometries. It was found that the flow structure and heat transport were dependent on aspect ratio, angle of tilt and Rayleigh number in a very complex way. Any correlation for Nusselt numbers in tilted geometries should reflect this complexity. An examination of the results obtained

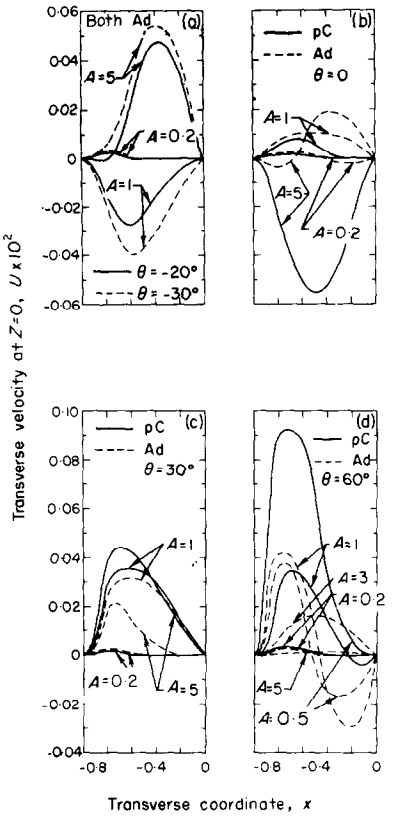

FIG. 11. Transverse velocity, u, at the cavity midplane, $z = 0$, for $R = 300\,000$.

here, in comparison with those of Dropkin and Somerscales, points to this fact. An attempt has not been made to express these results in terms of empirical fit correlations for this same reason.

The effect of sloping boundaries and the associated delineation of the conduction and boundary layer regimes in the fluid flow are discernible from an examination of the flow field results presented. It can be seen that with increasing Rayleigh numbers the heat transported by convective mechanisms, in comparison to that of conduction, is larger. Skewness of velocity profiles is ascribable not only to increasing shear layers near the wall with increasing Rayleigh numbers but also to the significant role played by the components of the gravitational field that serve as driving mechanisms. The limiting case of a tall, narrow slot yields essentially a cubic velocity profile. It is conjectured, therefore, that a stability analysis for large aspect ratio, based on a parallel flow model with adjustable parameters as done by Hart [2], should be capable of predicting transitions quite effectively.

The heat transport results for tilt angles where the top plate is hotter provide a new insight into the so-called convectively stable regime. It can be seen that a large transport of heat is associated with the convective mechanism even in this case. It is clear that thermal instabilities associated with regions of adverse temperature gradient, due to the presence of conducting end walls, should be possible even in the case of top heating. An investigation of these effects, which would be more pronounced for the case of finite Prandtl number situations, warrants further important study.

End wall effects are visible from an examination of the corresponding temperature and flow fields. For large aspect ratio, decreasing the aspect ratio induces a transverse fluid motion which serves to increase convective heat transport. The presence of the end walls also serves to inhibit longitudinal fluid motion, and for small enough aspect ratio these two mechanisms compensate each other resulting in a decrease in the overall heat transport. These compensating effects result in a maximum heat transport at some finite aspect ratio for all tilt angles.

Acknowledgements—This work is based in part on a Ph.D. thesis by P. S. Ayyaswamy carried out in the Morrin–Martenelli–Gier Heat Transfer Laboratory of the University of California, Los Angeles. Grateful acknowledgement is made for support by the National Science Foundation (Grant GK-35892) and for use of the UCLA Computing Center Facilities.

REFERENCES

1. P. S. Ayyaswamy, Natural convection flows in tilted configurations, Doctoral dissertation, University of California, Los Angeles (1971).
2. J. E. Hart, Stability of the flow in a differentially heated inclined box, *J. Fluid Mech.* **47**, 547–576 (1971).
3. G. K. Batchelor, Heat transfer by free convection across a closed cavity between vertical boundaries at different temperatures, *Q. Appl. Math.* **12**, 209–233 (1954).
4. A. E. Gill, The boundary-layer regime for convection in a rectangular cavity, *J. Fluid Mech.* **26**, 515–536 (1966).
5. J. W. Elder, Laminar free convection in a vertical slot, *J. Fluid Mech.* **23**, 77–98 (1965a).
6. J. W. Elder, Turbulent free convection in a vertical slot, *J. Fluid Mech.* **23**, 99–111 (1965b).
7. E. R. G. Eckert and W. O. Carlson, Natural convection in an air layer enclosed between two vertical plates with different temperatures, *Int. J. Heat Mass Transfer* **2**, 106–120 (1961).
8. A. F. Emery, The effect of a magnetic field upon the free convection of a conducting fluid, *J. Heat Transfer* **85**, 119–124 (1963).
9. G. Poots, Heat transfer by laminar free convection in enclosed plane gas layers, *Q. J. Mech. Appl. Math.* **11**, (3), 257–267 (1958).
10. G. deVahl Davis, Laminar natural convection in an

enclosed rectangular cavity, *Int. J. Heat Mass Transfer* **11**, 1675–1693 (1968).
11. A. Rubel and F. Landis, Numerical study of natural convection in a vertical rectangular enclosure, *Int. Symp. High Speed Computing in Fluid Dynamics*, The Physics of Fluids, Monterey (19–24 August 1968), New York, Am. Inst. Phys., pp. 208–213 (1969).
12. C. Quon, High Rayleigh number convection in an enclosure—A numerical study, *Physics Fluids* **15**, 12–19 (1972).
13. L. A. Segel, Distant side-walls cause slow amplitude modulation of cellular convection, *J. Fluid Mech.* **38** (1), 203–224 (1969).
14. R. Krishnamurti, Finite amplitude convection with changing mean temperature. Part 1, Theory. Part 2, Experimental test of theory, *J. Fluid Mech.* **33**, 445–463 (1968).
15. S. H. Davis, Convection in a box, *J. Fluid Mech.* **30**, 465–478 (1967).
16. I. Catton and D. K. Edwards, Effects of side walls on natural convection between horizontal plates heated from below, *J. Heat Transfer* **89C**, 295–299 (1967).
17. L. Prandtl, *Essentials of Fluid Dynamics*. Hafner, New York (1952).
18. G. Z. Gershuni, On the stability of plane convective motion of a fluid, *Zh. Tekh. Fiz.* **23** (10), 1838 (1953).
19. D. Dropkin and E. Somerscales, Heat transfer by natural convection in liquids confined by two parallel plates which are inclined at various angles with respect to the horizontal, *J. Heat Transfer* **87**, 77–84 (1965).
20. F. Landis, Referee discussion of [19]; *J. Heat Transfer* **87**, 77–84 (1965).
21. S. Chandrasekhar, *Hydrodynamic and Hydromagnetic Stability*. Clarendon, Oxford (1961).
22. U. H. Kurzweg, Stability of natural convection within an inclined channel, *J. Heat Transfer* **92C** (1), 190–191 (1970).
23. V. E. Denny, University of California, Los Angeles: personal communication.

CONVECTION NATURELLE DANS UNE FENTE FINIE ET RECTANGULAIRE, ARBITRAIREMENT ORIENTÉE PAR RAPPORT Á LA VERTICALE

Résumé —On a obtenu par la méthode de Galerkin les solutions des équations du mouvement permanent et bidimensionnel de convection naturelle d'un fluide de Boussinesq à grand nombre de Prandtl contenu dans une fente rectangulaire inclinée différentiellement chauffée. Le problème a été résolu pour des conditions aux limites de parois parfaitement conductrices ou adiabatiques. Les domaines de variation des paramètres sont les suivants : nombre de Rayleigh inférieur à $2 \cdot 10^6$, facteur de forme entre 0,2 et 20, angle de calage depuis $-30°$ (plaque inférieure la plus chaude) jusqu'à $+75°$ (plaque supérieure la plus chaude). Ces paramètres décrivent aussi bien les régimes de conduction que de couches limites. Les distributions calculées numériquement qui comprennent les écoulements multicellulaires, les profils de température et les flux thermiques s'accordent avec les résultats expérimentaux et avec d'autres études numériques.

NATÜRLICHE KONVEKTION IN EINEM ENDLICHEN, RECHTECKIGEN SPALT MIT BELIEBIGER ORIENTIERUNG IN BEZUG AUF DEN SCHWERKRAFTVEKTOR

Zusammenfassung—Lösungen der stationären, zweidimensionalen Bewegungsgleichungen, welche die natürliche Konvektion einer Boussinesq-Flüssigkeit grosser Prandtl-Zahl in einem differential geheizten, geneigten rechteckigen Spalt beschreiben, wurden mit der Galerkin-Methode erhalten. Das Problem wurde für vollkommen leitende und adiabate Randbedingungen an den Seitenstreifen gelöst. Der untersuchte Parameterbereich umfasst Rayleigh-Zahlen bis $2 \cdot 10^6$, Seitenverhältnisse zwischen 0,2 und 20 und Neigungswinkel zwischen $-30°$ (untere Platte beheizt) und $+75°$ (obere Platte beheizt). Diese Parameter beschreiben sowohl den Leitungs- als auch den Grenzschichtbereich. Die berechneten Strömungsverteilungen, einschliesslich dem Auftreten von Vielzellenströmungen, die Temperaturprofile und die Voraussage über den Wärmeübergang stimmen sehr gut mit experimentellen Ergebnissen und anderen numerischen Berechnungen überein.

СВОБОДНОКОНВЕКТИВНОЕ ТЕЧЕНИЕ В ЩЕЛИ ПРЯМОУГОЛЬНОГО СЕЧЕНИЯ КОНЕЧНЫХ РАЗМЕРОВ, ПРОИЗВОЛЬНО ОРИЕНТИРОВАННОЙ ОТНОСИТЕЛЬНО ВЕКТОРА СИЛЫ ТЯЖЕСТИ

Аннотация—Методом Галеркина получены решения стационарных двумерных уравнений движения, описывающих свободноконвективные течения жидкости Буссинеска при большом числе Прандтля в прямоугольной неравновесно нагреваемой наклонной щели. Задача решена для адиабатических граничных условий и для условий идеальной теплопроводности на кромках щели. Исследования проводились в следующих диапазонах параметров: число Релея до 2×10^6, относительная длина от 0,2 до 20; угол наклона от $-30°$ (нижняя пластина теплее) до $+75°$ (верхняя пластина теплее). Эти параметры описывают режимы теплопроводности и пограничного слоя. Рассчитанные распределения потока, включая возникновение многячестых потоков, профили температуры и коэффициенты теплообмена, хорошо согласуются с экспериментальными данными и другими численными расчетами.